Ecotoxicology and Environmental Safety 318 (2026) 120229

Contents lists available at ScienceDirect

Ecotoxicology and Environmental Safety

journal homepage: www.elsevier.com/locate/ecoenv

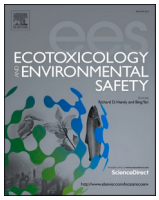

Identification method of asbestiform mineral particles and cleavage fragments in the lung: Regulated and unregulated amphiboles

Maxime Misseri [a,*], Sara De Salvo [b], Karine Beugnon [c], Tomas Danek [b], Catherine Verdun-Esquer [d], Camille Carles [d], Patrick Bontemps [b], judicaël Prieur [b], Jean-Claude Pairon [e,f], Laurent Martinon [c]

[a] Integrated Transformations of Renewable Matter (TIMR), University of Technology of Compiègne, Sorbonne University Alliance, Rue Roger Couttolenc, CS 60319, Compiègne 60203, France
[b] AD-LAB Asbestos Research Analysis Laboratory, 7, ZA du Plat du Pin, Brussieu 69690, France
[c] Asbestos Fibers and Particles Laboratory (LAFP), Environmental Health Laboratories Service (SLSE), 11 rue George Eastman, Paris 75013, France
[d] Occupational Health and Environment Department, Bordeaux University Hospital, Place Amélie Raba-Léon, Bordeaux 33000, France
[e] INSERM U955, GEIC20 team, Faculty of Health, 8, rue du Général Sarrail, Créteil 9400, France
[f] Occupational and Environmental Diseases Department, Intercommunal Hospital of Créteil (CHIC), 40 avenue de Verdun, Créteil cedex 94010, France

ARTICLE INFO

Keywords:
Lung cancer
Amphibole asbestos
Asbestos body
Cleavage fragment
Elongate mineral particle
TEM

ABSTRACT

Asbestos fibers are well-established causes of lung and pleural diseases. However, the role of other non-asbestiform elongate mineral particles (EMPs) in these conditions remains unclear. This study aimed to assess the feasibility of detecting exposure to EMPs, including non-asbestiform cleavage fragments, in individuals working in industries such as mining, quarrying, public works, construction, and agriculture, by analyzing the mineral lung burden. The study involved lung biopsies from 25 individuals: 20 with lung cancer and 5 with other lung diseases, all of whom had worked in the aforementioned sectors and had an asbestos body (AB) concentration greater than 1000 AB/g of dry lung tissue, the reference value above which ABs concentrations correspond to a non-trivial exposure to asbestos. An analytical protocol was developed to distinguish asbestiform fibers (both basal and apical parts) from two types of non-asbestiform cleavage fragments for both the coated and uncoated particles. Collected asbestos bodies (ABs) were treated with oxalic acid to partially dissolve their ferruginous coating, allowing for visual observation, crystallographic characterization, and chemical analysis via transmission electron microscopy (TEM). Results showed 44 amosite asbestos bodies, 3 crocidolite bodies, 1 ferro-actinolite body, and 6 grunerite non-asbestiform ferruginous bodies. Among 376 regulated and unregulated amphibole particles analyzed both coated and uncoated, 252 were asbestiform, 119 were cleavage fragments, and 5 were undetermined. Given the diversity of particle origins observed, their surface properties likely vary, which may influence their toxicity. It would therefore be important to include these particles in future studies of the mineral lung burden.

1. Introduction

1.1. Development of a new methodology

Workers in mining, quarrying, construction, and agricultural industries may be exposed to elongate mineral particles (EMP). The EMP refers to any mineral particle with an aspect ratio greater than 3 (NIOSH, Castellan et al., 2011). In a collective expert assessment, ANSES (French Agency for Food, Environmental and Occupational Health & Safety) has raised the question of the safety of certain EMPs. While it is clearly established that there is a link between asbestiform mineral particles (ASBs), particularly amphiboles, and certain lung diseases (lung cancer, pleural mesothelioma, asbestosis, pleural plaques, etc.) and other forms of cancer (laryngeal and ovarian cancers), epidemiological studies have not ruled out a health risk linked to exposure to cleavage fragments from non-asbestiform minerals (CFs) analogous to the five regulated asbestiform amphiboles: crocidolite (riebeckite), amosite (grunerite), tremolite, actinolite and anthophyllite (ANSES, 2015). “EMP of interest” are

* Corresponding author.
E-mail address: maxime.misseri@ad-lab.fr (M. Misseri).

https://doi.org/10.1016/j.ecoenv.2026.120229
Received 14 November 2025; Received in revised form 13 April 2026; Accepted 4 May 2026
Available online 13 May 2026

particles likely to be inhaled (width < 3 μm) from mineral species of interest such as ASB (regulated amphiboles and chrysotile), CF homologous to asbestos, and other types of minerals as winchite, richterite, fluoro-edenite and erionite (ANSES, 2015 and ANSES, 2017). Since we identified amphibole species in the lung burden extending beyond those listed by ANSES, the term EMP will be used exclusively throughout this article for all elongate amphibole particles detected.

EMP's biopersistence is poorly understood. If it is similar to that of asbestos amphibole fibers, they may constitute a potential risk factor for the development of respiratory diseases if inhaled (Pairon, 1996; Gualtieri, 2018; Okimoto et al.,2013; Gualtieri et al., 2018; Donaldson et al., 2013).

Broadly speaking, EMP toxicity is profoundly influenced by the structure of the mineral, as stated by (Gualtieri, 2018). A key question arises: do we have sufficient knowledge of the particles present in the pulmonary mineral deposits of individuals with lung conditions related to asbestos exposure?

In this exploratory study, the first objective was to develop a new method of identifying the mineral in question with greater precision, as well as its crystalline habitus crystal morphology), whether particles were coated or uncoated. This identification constitutes a crucial step in categorizing biopersistent EMP, the potential toxicity of which requires assessment, by using indices such as the Fiber Potential Toxicity/Pathogenicity Index (FPTI) proposed by Gualtieri (2018).

1.2. Particles in the lung parenchymal tissues

The second objective of the study was to apply this new analytical method to particles likely to be present in large quantities in the lung parenchymal tissues of a series of 25 selected subjects.

The challenge was to investigate, in patients with lung conditions usually attributed to asbestos and who had worked in the mining and quarrying, construction, or agricultural sectors, whether some of the asbestos bodies contained in their lungs had formed around non-asbestiform EMP. In other words, could non-asbestiform EMP cause lung conditions usually attributed to ASBs?

Inhaled fibers may undergo phagocytosis by alveolar macrophages, which can lead to the formation of ferruginous bodies (FBs) (Gross et al., 1967). When the fibers in question are ASBs, these FBs are referred to as asbestos bodies (ABs) (Gloyne, 1931 and Bignon et al., 1970).

Two markers can be used to characterize abnormal retention of ASBs in the lungs: ABs, which are ASBs coated in hemosiderin and which are observed (Brouet et al., 1967) and counted using optical microscopy (Craighead, Mossman, 1982) and uncoated ASBs, detected and counted using electron microscopy (Capella et al., 2016; Rasmuson et al., 2014 and Visonà et al., 2022). For example, measuring the asbestos lung burden through electron microscopy shows a strong correlation with the presence of pleural plaques in patients with mesothelioma (Visonà et al., 2023).

Based on a selection of patients in whom clinicians had diagnosed an asbestos-related condition and for whom lung biopsy analysis showed higher-than-normal retention of asbestos bodies, a parenchymal sample preparation protocol was developed in the laboratory to partially dissolve the ferruginous coating surrounding the particles forming the ABs or non-asbestos ferruginous bodies NAFBs. By removing sufficiently large sections of particles from their coatings, visual observations, quantitative electron diffraction analyses, and chemical analyses were possible during transmission electron microscopy (TEM) analysis. Visual observations combined with a flowchart based on the latest research on the nucleation of ASBs (Misseri, 2023) made it possible to characterize and differentiate between CFs and ASBs. The same analyses were performed on uncoated amphiboles.

1.3. State of the art and terminology of amphibole particles

This study focuses on amphiboles, as the non-asbestiform analogues of chrysotile, antigorite and polygonal serpentine, are easy to characterize.

Scientific literature regarding particles derived from asbestiform and prismatic (or acicular) amphiboles is traditionally structured around a binary dichotomy: ASBs versus CFs. Several reviews have addressed this issue (Ilgren, 2004; Militello et al., 2021; Goodman et al., 2023).

- Asbestiform habit: This refers to a mineral morphology that has naturally crystallized in a manner that allows it to be easily separated into long, thin, flexible, and strong fibers.
- Non-asbestiform habit: This refers to growth forms that produce CFs when fragmented by mechanical force. These particles do not separate easily from the massive mineral, lack tensile strength, and are not flexible. They do not possess the intrinsic characteristics of naturally formed ASBs (Veblen, Wylie, 1993).

While asbestiform and non-asbestiform EMPs differ primarily in their morphology, they are chemically indistinguishable (Ilgren, 2004; Militello et al., 2021).

In nature, asbestiform amphiboles (NOA, for *Naturally Occurring Asbestos*) form through unidirectional growth. Geologically, it is possible to find minerals that form through unidirectional growth when a saturated, pressurized geofluid is forced into a pressure-deficient cavity, such as a fracture, lava vesicle, or pressure shadow. In general, they crystallize from chemical elements derived from the dissolution of non-asbestiform amphiboles of identical chemical composition, driven by hydrothermal fluids circulating along fracture walls. This process occurs within a complex geological context defined by cycles of fracturing, micro-fissuring, and abrupt variations in hydrostatic pressure. Near the fractures, these amphiboles are also found within microcavities. The appearance of these microcavities precedes the opening of the fractures.

A careful examination of the contact zones between asbestiform and non-asbestiform facies reveals the presence of amphiboles with intermediate characteristics associated with asbestos formation. These amphiboles are capable of generating chemically identical EMPs exhibiting some distinct morphological and physical properties (Misseri, 2023).

Anthropogenic actions performed on these rocks release a mixture of asbestiform amphiboles (referred to as Apical Part of Asbestos Mineral APAM in this article) and CFs (referred to as FRAG). However, two specific types of EMPs complete this inventory:

- Developing Sub-Grains (DSG): These are sub-grains of prismatic or acicular amphiboles that have been thinned and detached lengthwise from the primary mineral by the leaching of hydrothermal fluids. Although they generally remain attached to the primary mineral at their base—justifying their classification as CFs—they exhibit a much higher aspect ratio and greater fragility than classic CFs. They have been subjected to numerous micro seismic stresses that can lead to microcracks.
- Base Part of Asbestiform Minerals (BPAM): These particles originate from the base of asbestiform minerals. They are formed by unidirectional growth. They have been subjected to micro-seismic stresses resulting in potential micro-cracks. While their appearance is similar to APAM, they are thicker and more fragile. They exhibit a specific fracture pattern, and their ends may reveal the beginnings of growth of finer-diameter fibers organized into bundles. Their dimensions are largely similar to DSGs; however, they can be much thinner and possess a higher aspect ratio.

2. Sampling and methodology

2.1. Case selection

The study was conducted on a group of 25 subjects, including 20 with bronchopulmonary cancer and 5 with pleural plaques, diffuse interstitial fibrosis and pleurisy. All had worked in sectors such mining,

quarrying, construction, roadwork, or agriculture, all these sectors comprising a risk of dusts exposure with a strong probability to inhale amphiboles in both asbestiform and non-asbestiform habits.

These subjects were selected due to the presence of a significative or high concentration of ABs in lung tissue greater than 1000 ABs/g (Churg, 1982 and De Vuyst et al.,1998) of dry tissue detected by optical microscopy. This reference value is the threshold value defined from a reference population without any exposure to asbestos (white-collars), above which ABs concentrations correspond to a non-trivial exposure to asbestos (De Vuyst et al., 1998). This selection criterion was intended to ensure that the analyzed samples reflected significant exposure to EMPs, thereby allowing for an effective evaluation of the analytical protocol developed.

As the participants in this study had long professional careers, some of them were exposed to environmental and industrial pollutants (Table 1). Industrial pollutants, such as crocidolite and amosite, are easily identifiable: their chemical composition, in particular, allows them to be traced back to the amphiboles extracted from the main exporting mine. This correlation also applies to tremolite and anthophyllite, which are known to have contaminated the mineral load of certain products. In contrast, actinolite, (Baumann, Lacas, 2014) frequently detected in outdoor air during routine analyses in mainland France, is mostly linked to natural occurrence. It should therefore be considered an environmental EMP marker, similarly to unregulated amphiboles.

This ambiguity does not introduce any major bias into the present study, the objective of which is to characterize all types of EMPs. Consequently, this study was not designed to isolate the specific amphiboles within the detected mixtures responsible for the observed pathologies. Future research utilizing targeted cohorts and alternative protocols should address this question.

Table 1
Occupational histories of subjects with possible exposure to industrial or environmental elongate amphibole particles, professions classified by type of amphibole exposure, BPW = Building and Public Works / Construction industry). "—" indicates no recorded exposure in this category, ID=project number.

ID	Possible exposure to actinolite, tremolite and other naturally occurring amphiboles	Possible exposure to industrial crocidolite and amosite, or tremolite / anthophyllite contaminating mineral fillers
4	Miner	Electrician
6	Miner, gardener	—
7	Miner	Power plant worker
8	Miner	Furnace maintenance in a steelwork
2	Miner	Asbestos products manufacturing
3	Agricultural worker, construction (BPW), mason, concrete mixer operator	Tiler, boiler demolition
5	Agricultural worker	Heating installer
10	Agricultural worker, kerb stone layer, mason	Tiler, fibre-cement pipe cutting
18	Agricultural worker, mason, concrete mixer operator	Heating installer / boiler operator
23	Agricultural worker, construction (BPW), mason	Demolition worker (fibre-cement pipe installation)
9	Quarry worker	—
13	Quarry worker	Boilermaker
14	Quarry worker	blowtorch cutter worker
15	Quarry worker	—
16	Quarry worker	—
1	Earthworker, mason	Brickmaker, roofer, fibre-cement cutter
11	Earthworker, construction (BPW), mason, memorial stone installer	—
12	Earthwàrker, construction (BPW)	Painter
19	Earthworker, mason	Pipefitter
17	Construction (BPW)	Painter and brake lining replacement
20	Construction (BPW), mason	—
21	Construction (BPW), mason	Brickmaker
22	Construction (BPW), mason	Welder, vehicle body repairer, metal frame worker
24	Construction (BPW)	Demolition worker
25	Construction (BPW)	scrap metal worker

Samples were collected according to the guidelines of the European Respiratory Society (ERS) (De Vuyst et al., 1998) by two public by the Intercommunal Hospital of Créteil (CHIC) and the Bordeaux University Hospital - Pellegrin Hospital and transmitted to the asbestos fibers and particles laboratory (LAFP) for mineralogical analysis by optical microscopy. Selection was made from the LAFP samples base.

The health data and parenchymal samples used to conduct the study were derived from research promoted by the IIMTPIF (the Interuniversity Institute of Occupational Medicine of Paris Ile-de-France) on a "Molecular Approach for the Evaluation of the Relationship Between Exposure to Fibrous Mineral Particles and the Occurrence of Lung and Pleural Lesions in Humans", conducted on patients with lung cancer or mesothelioma between 2005 and 2008. This research was approved by a Consultative Committee for the Protection of Individuals in Biomedical Research (CCPPRB Créteil-Henri Mondor) examined during the session of March 14, 2005 n°05–005.

2.2. Preparation

A protocol combining the preparation method for LAFP biometrological analysis with the methods of Dumortier, De Vuyst, (1988) and Dodson et al., (1983) was implemented as part of this study. This protocol enhances the likelihood of relocating particles initially observed under an optical microscope to the grids used for (TEM). Before observation under an optical microscope and transfer to the electron microscopy grid, the filter on which the particles were collected was treated with oxalic acid at 50°C. This treatment partially dissolves the ferruginous coating surrounding the EMP. Thus, while the ABs partially released from their coating remain observable under the optical microscope, their sections freed from the coating, if sufficiently large, allow for visual observations, quantitative electron diffraction, and chemical analyses during TEM analysis.

The samples were weighed on a precision scale. The test sample was adjusted (between approximately 10 and 30 mg dry weight) based on the asbestos body concentration measured initially to ensure there were neither too many nor too few objects to identify. The lung tissue was then digested with sodium hypochlorite at 9.6% active chlorine (approximately 6 ml per 100 mg of wet tissue) and filtered through a 3 μm porosity Millipore membrane. This membrane was placed in a filter holder through which 40 ml of 8% oxalic acid (11.2 mg in 100 ml of ultrapure water) was passed to partially release the asbestos bodies from their ferruginous coating. The filter holder was then heated at 50°C in a water bath for 4 h. The filter was rinsed with 100 ml of ultrapure water (at the same temperature as the water bath) and then placed in an oven at 60°C for approximately 15 min. Once completely dry, the filter was placed on a glass optical microscope slide onto which acetone was sprayed to make the filter transparent and polymerize it.

The filter was then observed under an optical microscope at a magnification of X200 to look for ABs or NAFBs that had been more or less released from their ferruginous coating by oxalic acid.

When a coated particle was observed, it was "marked" with a pointer so that its position could be determined. A layer of carbon was then sprayed onto the slide using a carbon evaporator. Then the membrane fragment with the coated particle was cut out using a scalpel under a binocular microscope and transferred to a pre-carbonated copper electron microscopy grid using the Jaffe washer method, substituting acetone for chloroform.

2.3. Analyses

The entire grid was then observed at a magnification between X11,500 and X15,000.

TEM-EDS analyses were performed using an FEI CM120 operating at an accelerating voltage of 120 kV, equipped with a Samx Numer-iX+ EDS. The target and the microscope measurement function, required for particle length and width measurements, were connected using SPI microspheres and an Agar Scientific S106 cross grating. The microanalysis system was verified using standard minerals and 1867a reference materials, with a maximum permissible error of 10% per element on the finest particles. The diffraction measurement function was calibrated using the SPI gold standard.

2.4. Verification of the impact of the preparation on amphibole chemistry

The preparation protocol used oxalic acid. It was verified that the oxalic acid treatment did not alter the chemistry of the particles. This verification was performed using three asbestos standards: one for tremolite, an environmental asbestos, and two for crocidolite and amosite, industrial asbestos. The standards used were those of the HSE (Health and Safety Executive, UK) and the IOM (Institute of Occupational Medicine, Edinburgh).

The tremolite was from the Saltworks mine in California, USA.

The amosite was from the Penge mine in South Africa.

The crocidolite was from the Coretsi mine in Kuruman, South Africa.

The average of the ten measurements taken for each asbestos standard treated with oxalic acid was compared (Fig. 1) with the values for these asbestos standards provided in the literature:

- The tremolite average with the chemical composition provided by Jung et al., (2021);
- The crocidolite average with the average of the chemical compositions of crocidolites from Kuruman in South Africa, provided by Shedd, (1985);
- The amosite average with the average of the chemical compositions of amosites from the Penge mine in South Africa and provided by several authors (Ballirano et al., 2022; Germine and Puffer, 2020; Kohyama et al., 1996; Bowes and Farrow, 1997 and Pollastri et al., 2015).

The measurements showed that the use of oxalic acid in processing did not alter the chemical compositions of ASBs.

2.5. Identification from a chemical measurement

Chemical analysis performed by EDS coupled with TEM should enable the analysis of very fine particles - the finest ASB are approximately 20 nm in diameter (Millette, Compton, 2005) - with a variation per element not exceeding 10%. In mineralogy, the classification of amphiboles has been established from measurements carried out on larger minerals than the EMP is using an Electron Probe Microanalyzer (EPMA) (Veblen, Ribbe, 1982) with an accuracy of around 1%. EPMA analyses are possible on particles larger than 3–4 μm, which are unlikely to reach the deep lung. Therefore, EPMA is not a suitable analytical method for the identification of NOA (Naturally Occurring Asbestos). The accuracy of EDS coupled with TEM is sufficient for identifying amphibole asbestos that have been intentionally added to building materials, as their characteristics are well known. This is not the case with naturally occurring amphibole asbestos (Ray, 2021).

Due to the 10% element-specific uncertainty for the finest fibers analyzed with EDS (the method is semi-quantitative), the calculated structural formula of the mineral may exhibit an imbalance. For example, this may manifest as a deficiency of an element in a specific site of the typical amphibole molecule. The single chemical analysis obtained with EDS on a mineral particle can be optimized. This optimization consists of searching for the chemical composition of the

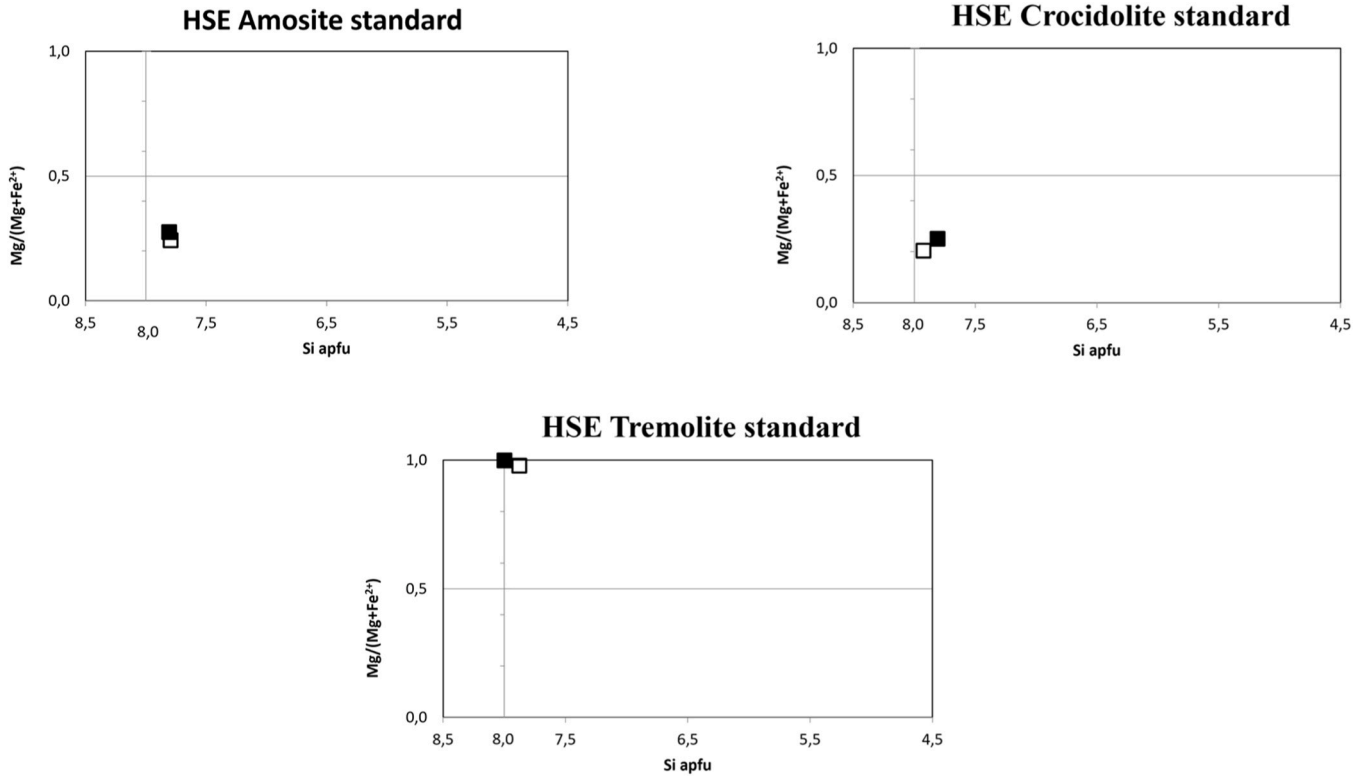

Fig. 1. Comparison of the average of 10 measurements taken for each HSE/IOM tremolite, crocidolite, and amosite standard with literature measurements for these asbestos standards, using compositional diagram. The horizontal axis corresponds to the number of silica atoms per formula unit (apfu), and the vertical axis corresponds to the number of magnesium (apfu) over the sum of the number of magnesium (apfu) and the number of ferrous iron (apfu). The empty squares correspond to the averages of the 10 measurements taken on the HSE standards treated with oxalic acid, and the filled squares correspond to the literature values.

theoretical amphibole that is closest to the detected particle, while remaining within the measurement uncertainty. When this optimization is possible, the resulting structural formula can then be used to make relevant comparisons with existing mineralogical or geological data. This methodological approach was used for the accurate identification of amphiboles in our study. The structural formulas of amphiboles were calculated using the Excel spreadsheet (version 1.9.8) (Locock, 2014) which allows amphiboles to be identified according to the nomenclature recommended by the International Mineralogical Association - IMA 12 (Hawthorne et al., 2012).

2.6. Identification using quantitative diffraction

Quantitative diffraction can be used to measure inter-reticular distances. This enables a mineral to be identified based on the specifics of its crystalline structure. Anthophyllite and cummingtonite are amphiboles that share the same chemistry; only their crystalline structures differ. Whenever possible, quantitative diffraction was used to identify anthophyllite.

Diffraction was also used to identify polygonal serpentine, which has the same chemistry as chrysotile and fibrous antigorite.

2.7. Characterization of particle type

As early as the 1980s, several seminal studies (Campbell et al., 1980; Siegrist and Wylie, 1980; Shedd, 1985) proposed the use of particle dimensions as a discriminant criterion to distinguish ASB from CFs. This dimensional approach has been continually refined over the decades. Harper et al. (2012) suggested that a width threshold of less than 1 μm effectively encompasses ASBs while minimizing the inclusion of CFs; however, the authors clarified that this criterion does not represent a strict boundary between safety and pathogenicity.

Subsequently, based on observations of AB and amphiboles within pulmonary mineral burdens, Roggli, Green, (2019)) defined specific morphometric criteria for differentiation: a minimum length of 10 μm combined with a diameter of less than 1.0 μm. These conclusions were challenged by Finkelstein (2019), who drew upon Harper et al., (2008)) regarding the granulometric evolution of particles, from the parent rock to their dispersion following mechanical stress.

In parallel, alternative protocols have emerged to enhance discrimination. Chatfield (2018) developed a method based on the joint distribution of aspect ratio and width for respirable elongate mineral particles (EMPs) longer than 5 μm. More recently, Wylie et al. (2022) established a robust mathematical and statistical discriminant function derived from an extensive inter-laboratory dataset. This work was further extended by Korchevskiy and Wylie (2025), who linked analytical discrimination to the estimation of the particles' carcinogenic potential.

However, these statistical methods prove difficult to apply when samples contain low particle concentrations. To address this limitation, approaches based on the qualitative description of the asbestiform habit were developed alongside dimensional criteria, following the pioneering work of Langer et al. (1991) and the subsequent decision flowcharts of Van Orden et al. (2008). In continuation of this research and following the identification of intermediate EMPs (such as DSG and BPAM) that predominantly occupy the dimensional overlap zone, the MBP2022 flowchart was developed to optimize the classification of particles falling within this overlap zone.

The initial objective was to test the flowchart called “MB2015” which was developed according to criteria set out in the scientific literature (Misseri and Billon-Galland, 2021). However, research conducted from 2021 to 2022 by University of Technology of Compiègne reviewing has contributed substantially to an increased understanding of the nucleation of asbestiform calcium amphiboles. On the one hand, this study confirms that asbestiform minerals crystallize according to the Vapor, Liquid, Cristal (Givargizov, 1973) mechanism or Vapor, Liquid, Solid (VLS) a similar mechanism (Wagner, Ellis, 1965), a hypothesis previously put forward by mineralogists (Veblen and Ribbe, 1981; Sunagawa et al., 2005). On the other hand, this new understanding of the boundary between asbestiform minerals and amphiboles altered by hydrothermal fluids (Misseri, 2023) led to a complete review of MB2015, resulting in an updated version, the MBP2022 flowchart which is described in this article.

Visual observations made it possible to characterize CFs and ASBs. Four types of EMP were considered:

- CFs from unaltered amphiboles (FRAG), generally lacking parallel edges.
- Developing SubGrain (DSG) fragments, from amphiboles leaching by the circulation of hydrothermal fluids along the cleavages. These CFs generally have parallel edges.
- Basal Part of Asbestos Mineral (BPAM) particles, from the basal part of asbestiform minerals formed by epitaxy through a VLC (or VLS) mechanism. Epitaxy is a layer-by-layer crystalline growth process. The organization of the molecular or atomic entities in the layers is determined by the lattice of an underlying crystal matrix. These particles have subparallel to conical edges. They are subcylindrical. This may be due to less development of the (110) faces of the particle. They may be finer than DSGs and fracture looks like conchoidally.
- APAM (Apical Part of Asbestos Mineral) particles, from the apical part of asbestiform minerals. APAM particles are very long and very thin, with parallel edges.

In the MBP2022 flowchart (Fig. 2), particles with non-parallel edges or without a slightly conical appearance are classified as CFs FRAG-type. The upper part of the MBP2022 flowchart is a differentiation based on particle dimensions. Particles with a width greater than 3 μm are classified as CFs (FRAG). A small number of particles with BPAM characteristics can conventionally be classified as CFs. Particles with a length-to-width aspect ratio greater than 20 are classified as APAMs. A small number of particles with DSG or BPAM characteristics can conventionally be classified as APAMs. The lower part of the MBP2022 flowchart

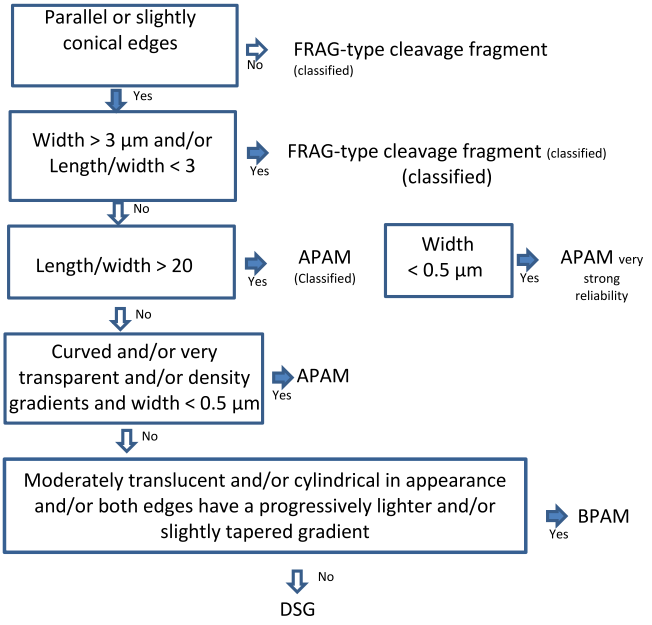

Fig. 2. MBP2022 flowchart to differentiate between the different elongate amphibole particles. APAM = particle from the apical part of an asbestiform mineral; BPAM = particle from the basal part of an asbestiform mineral, DSG = cleavage fragment from an altered mineral, FRAG = cleavage fragment from an unaltered amphibole.

differentiates particles with a width less than 3 μm and an aspect ratio less than 20 based on morphological criteria and criteria specific to transmission electron microscopy. Particles that have a curved shape and/or are transparent and/or exhibit electron density gradients and a width of less than 0.5 μm are identified as APAMs. Particles that do not exhibit these characteristics but are moderately translucent and/or have a cylindrical appearance and/or have both edges with an increasingly lighter gradient and/or are slightly conical are identified as BPAMs. Particles without any of these characteristics are identified as DSGs.

2.8. Validation of the MBP 2022 flowchart

An initial characterization phase was conducted on 200 particles from four reference standards (NIST SRM 1866 and 1867). The objective was to verify the MBP2022 flowchart's ability to discriminate particles based on their morphology. In accordance with the literature (Van Orden, 2008; Chatfield, 2023; Misseri and Billon-Galland, 2021), the tremolite and actinolite standards (SRM 1867) are primarily composed of non-asbestiform EMPs. Conversely, crocidolite and amosite (SRM 1866) contain a high proportion of ASBs. The results obtained (Table 2) corroborate these findings.

In a second stage, the efficiency and reproducibility of the MBP2022 flowchart were tested through a blind analysis. A sample of 150 randomized photographs—including sub-samples of crocidolite, amosite SRM standards and altered amphibolite (from the Sechilienne formation, Alps)—was submitted to three analysts. The results (Table 3), showing a 98% success rate, confirm the robustness of the tool and its consistency with initial observations.

The consistency of CF counting was evaluated by comparing (Table 4) the Van Orden flowchart (n = 100; Misseri and Billon-Galland, 2021) with the MBP2022 Flowchart (n = 200) using TEM images. Although derived from distinct sub-samples, both datasets originate from identical NIST SRM standards, ensuring the validity of the comparison (Kruskal-Walli's test). No significant difference was observed for amosite and tremolite ($p = 0.06$ and 0.35, respectively). In contrast, a highly significant difference was found for actinolite SRM 1867 ($p < 0.001$), with the Van Orden algorithm classifying 97% of particles as CFs compared to 53% for the MBP2022 Flowchart. This latter value aligns closely with EPA PLM data (49%) and the macroscopic appearance of the sample. This difference is largely attributable to the high proportion of BPAM (38%) in this sample, which exhibit conical or irregular ends. The Van Orden flowchart tends to classify these specific morphological features as CFs more frequently. The MBP2022 Flowchart addresses this limitation through a more nuanced analysis of fiber ends (conical/irregular vs. blunt/straight), thereby enhancing classification specificity, particularly for samples containing numerous intermediate morphologies (DSG, BPAM).

2.9. Statistical analysis

To ensure a diversity of perspectives and expertise, which is essential in a complex field such as amphibole particle characterization, five evaluators from three different laboratories were selected. This sampling made it possible to avoid biases related to choices guided by a single community of thought and encouraged the application of statistical tests measuring the concordance between evaluators' judgments. The five evaluators were tasked with characterizing the observed amphibole particles based on their photographs and dimensions.

To assess the degree of concordance between the participants' choices, three statistical tests were applied:

1.Cohen's kappa (McHugh, 2012): This test was performed by comparing the results of each pair of participants. It was used to measure the reliability of qualitative judgments between two evaluators, while taking into account chance agreements. Cohen's Kappa values are interpreted according to the Landis and Koch, (1977)scale:

- < 0: Disagreement.
- 0.01–0.20: Weak agreement.
- 0.21–0.40: Moderate agreement.
- 0.41–0.60: Average agreement.
- 0.61–0.80: Substantial agreement.
- 0.81–1.00: Almost perfect agreement.

2.Fleiss (1971): This test was also used in this context, as it is particularly suited to situations where multiple evaluators must classify items into qualitative categories. Fleiss's kappa values are interpreted similarly to those of Cohen's kappa.

3.Percentage agreement test: This last test measures the proportion of agreement between evaluators, providing an additional perspective on the concordance of judgments. It is used in conjunction with kappa tests to provide a more comprehensive overview of agreement between participants.

The MBP2022 flowchart, tested for its efficacy and reproducibility by three analysts, achieved a Fleiss's kappa of 0.91 and a percentage agreement of 0.98.

3. Results

A total of 479 mineral particles were observed in the 25 parenchyma samples. Among these particles, 376 amphiboles were counted, 56 of which were coated, along with other mineral particles, including 99 non-fibrous talc particles and one polygonal serpentine particle.

The focus was on all amphibole particles (Fig. 3) present: coated or uncoated, derived from CFs or ASBs and unregulated or regulated. In each amphibole family (see Table 5), CFs were detected, with a total of 119 for 252 particles derived from asbestiform minerals. Only 2 coated particles could not be characterized (dissolution of the coating was insufficient), and the habitus of three uncoated amphiboles could not be defined (one corresponded to contact between an altered amphibole and an asbestiform mineral, another was covered with a piece of carbon film that hindered its characterization, and the dimensions of the last one could not be recorded). All regulated amphiboles were observed (amosite, crocidolite, anthophyllite, tremolite, and actinolite), and 43 amphibole particles belonging to 6 unregulated amphibole species were observed (ferro-actinolite, magnesio-hornblende, magnesio-ferri-hornblende, edenite, and incidentally, one ferro-anthophyllite and one

Table 2
Determination of habitus of particles from NIST SRM asbestos standards with MBP2022 flowchart, APAM = particle from the apical part of an asbestiform mineral; BPAM = particle from the basal part of an asbestiform mineral, DSG = cleavage fragment from an altered mineral, FRAG = cleavage fragment from an unaltered amphibole, CF = total of cleavage fragments, ASB = total of asbestos mineral particles; WSI = Wilson Score Interval.

Particle	Crocidolite SRM 1866 en %	WSI en %		Amosite SRM 1866 en %	WSI en %		Actinolite SRM 1867 en %	WSI en %		Trémolite SRM 1867 en %	WSI en %	
FRAG	0	0	1.9	2	0.8	5	0	0	1,9	3	1.4	6.4
DSG	4	2	7.7	10	6.6	14.9	53	46	59.8	69	62.3	75
BPAM	3	1.4	6.4	9	5.8	13.8	38	31.6	44.9	24	18.6	30.4
APAM	93	88.6	95.8	79	72.8	84	9	5.8	13.8	4	2	7.7
CF	4	2	7.7	12	8.2	17.2	53	46	59.8	72	65.4	77.8
ASB	96	92.3	98	88	82.8	91.8	47	40.2	53.9	28	22.2	34.6

Table 3
A blind analysis of 150 random photographs, taken by 3 evaluators, which included crocidolite and amosite particles SRM standards and altered amphibolite, APAM = particle from the apical part of an asbestiform amphibole; BPAM = particle from the basal part of an asbestiform mineral, DSG = cleavage fragment from an altered amphibole, FRAG = cleavage fragment from an unaltered amphibole, CF = total of cleavage fragments, ASB. = total of asbestos mineral particles; WSI = Wilson Score Interval.

Particle	Crocidolite SRM 1866 en %	WSI en %		Actinolite SRM 1867 en %	WSI en %		ALP Amphibolite	WSI en %	
FRAG	0	0.0	7.1	0	0,0	7.1	60	46.2	72.4
DSG	4	1.4	9.4	52	38.5	65.2	40	27.6	53.8
BPAM	2	0.1	10.5	40	27.6	53.8	0	0.0	7.1
APAM	94	83.8	98	8	3.2	18.8	0	0,0	7.1
CF	4	1.4	9.4	52	38.5	65.2	100	92.9	100
ASB	96	86.6	99	48	34.8	61.5	0	0,0	7.1

Table 4
Cleavage fragment counting conducted on NIST SRM asbestos standards using: TEM Transmission electron microscopy (with Van Orden and MBP2022 flowcharts) and PLM polarized light microscopy (following criteria of EPA U.S. Environmental Protection Agency 1993), WSI = Wilson Score Interval.

	Amosite SRM 1866 en %	WSI en %		Trémolite SRM 1867 en %	WSI en %		Actinolite SRM 1867 en %	WSI en %	
Van Orden TEM	1	0.2	5.5	79	70.2	85.8	97	91.6	99.0
MBP2022 TEM	12	8.20	17.2	72	65.4	77.8	53	46.1	59.8
EPA 1993 PLM	13	7.8	20.0	53	43.3	62.6	49	39.4	58.7

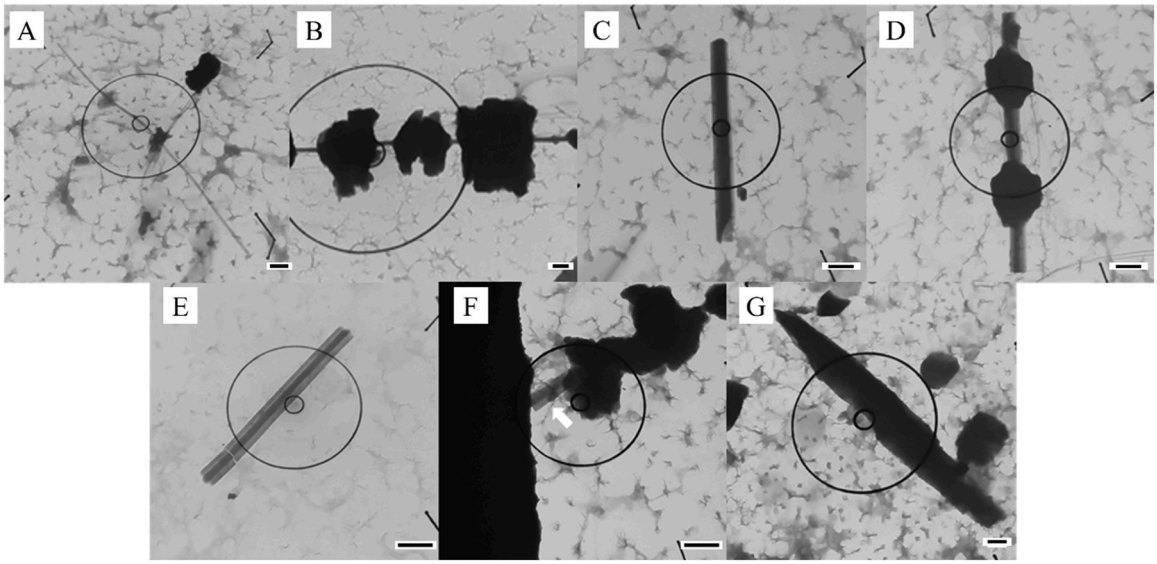

Fig. 3. Example of amphibole particles observed in the parenchyma. These are amosite-grunerite (A, B, C, D, E, and F) and an actinolite (G). The scale is provided by the bar, which is equal to 1 μm. Particles (B, D, and F) are coated particles. Particles A, B, C, and D are derived from asbestiform minerals: APAM = particle from the apical part of an asbestiform mineral (A and B) and BPAM = particle from the basal part of an asbestiform mineral (C and D). Particles E, F, and G are cleavage fragments: DSG = cleavage fragment from an altered mineral (E and F) and FRAG = cleavage fragment from an unaltered amphibole (G). In image F, the arrow indicates the exposed segment of the coated particle. B and D are Asbestiform Bodies (ABs). (F) is a Non-asbestiform Ferruginous Body (NAFB).

magnesio-riebeckite). Twenty-four of these unregulated amphibole particles were uncoated CFs. No coated or uncoated chrysotile fibers were observed. The CF of the magnesio-riebeckite particle possibly corresponded to Bolivian crocidolite.

The results of the three concordance tests were as follows: the average Cohen's kappa was 0.72, indicating substantial agreement; Fleiss's kappa was 0.71 indicating substantial agreement; the percent agreement was 92%. Overall, the agreement between the participants in the intercomparison process between the three laboratories was considered satisfactory. However, the Cohen's and Fleiss kappa results showed that the evaluators' experience significantly influenced their choices, despite the existence of a reference flowchart. Where there was disagreement, the characterization selected was the one that received the most approval.

For each type of amphibole, CFs and ASBs were observed. The distinction lies primarily in their respective proportions. The industrial amosite (grunerite) and crocidolite (riebeckite) contained the fewest CFs (Fig. 4).

Regarding coated particles (ABs and NAFBs), preparation of the samples enabled TEM observation of the mineral part at the center of the body. Defining criteria applicable to the mineral part during TEM analysis, as defined in this study (Fig. 2), made it possible to determine whether the particles were derived from asbestiform minerals or are CFs.

This allowed for the identification of 56 coated particles among the 25 samples examined using elemental chemical analysis and quantitative diffraction. Only 2 coated particles could not be characterized because the coating had not been sufficiently dissolved. Among the characterized particles, 44 were derived from amosite and 3 from crocidolite asbestiform minerals (APAM + BPAM). These were ABs formed around regulated asbestos. One particle originated from a ferro-

Table 5
amphibole particle types detected (coated or uncoated).

Particle from an asbestiform mineral/ AB	Cleavage fragment/NAFB	Potential source
Amosite***/AB	Grunerite /NAFB	Industrial minerals in general*
Crocidolite***/AB	Riebeckite	
Asbestos anthophyllite ***	Anthophyllite	Generally, amphiboles polluting industrial minerals** or naturally occurring in raw materials
Asbestos tremolite***	Tremolite	
Asbestos actinolite***	Actinolite	Generally, minerals naturally occurring in raw materials
Asbestiform ferro-actinolite/AB	Ferro-actinolite	
Asbestiform edenite	Edenite	
Asbestiform magnesio-hornblende	Magnesio-hornblende	
Asbestiform magnesio-ferri-hornblende	Magnesio-ferri-hornblende	

AB = Asbestos Body, NAFB = Non-Asbestiform Ferruginous Body.
* Industrial minerals are natural, non-metallic, non-energy raw materials formed in specific geological environments and extracted from the Earth's crust for their physical and chemical properties (French National Union of Quarrying and Materials Industries)
** pollutant of chrysotile, talc, and vermiculite - raw materials that are often imported
*** regulated

actinolite asbestiform mineral, thus forming an AB around an unregulated amphibole. Six were identified as grunerite CFs (DSG + FRAG) and therefore NAFBs.

Regarding particle width of coated and uncoated particles (Table 6), crocidolite-riebeckite, tremolite, and amosite-grunerite had the smallest widths, ranging from 0.06 to 1.25 μm, with medians between 0.18 and 0.41 μm. The widths of the other particles ranged from 0.13 to 2.29 μm, with medians between 0.56 and 1 μm.

The widths of amosite-grunerite, crocidolite-riebeckite, and tremolite showed a unimodal distribution (Fig. 5), while this distribution was polymodal for actinolite, ferro-actinolite, anthophyllite, edenite, magnesio-hornblende and magnesio-ferri-hornblende (Fig. 6).

4. Discussion

4.1. Application of the method

Only iron-rich amphiboles were identified as ABs (amosite, crocidolite, and ferro-actinolite) and NAFBs (grunerite). It is surprising, given the number of tremolite particles observed (71), that no coated particles were detected involving this type of amphibole. Tremolites at the core of ABs have previously been reported in the literature (Moulin et al., 1988 and Kohyama et al., 2017). Coated anthophyllites (Roggli and Green, 2019 and Holmes and Morgan, 1980) and coated actinolites (Roggli and Green, 2019) have also been reported. It is possible that the coatings are

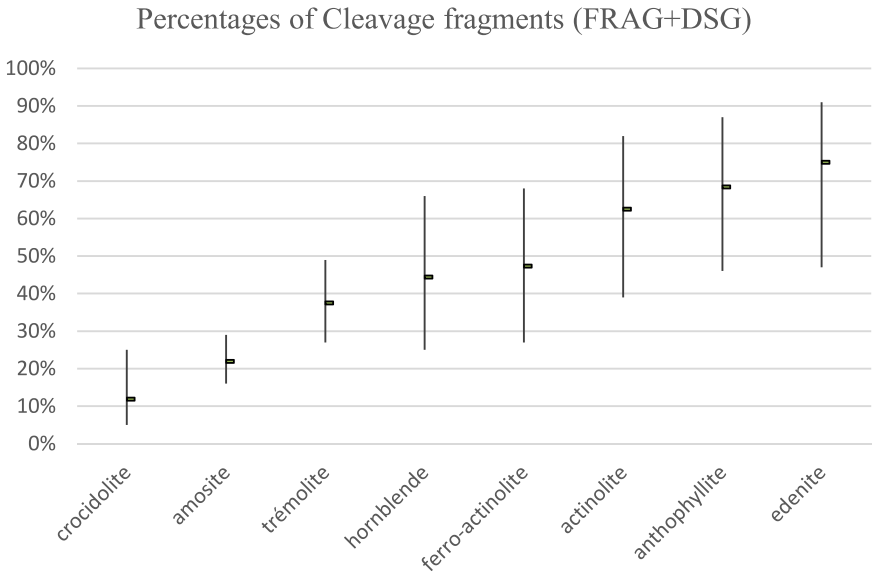

Fig. 4. Percentages of cleavage fragments (FRAG = cleavage fragment from an unaltered amphibole +DSG = cleavage fragment from an altered amphibole) by amphibole type, hornblende=Magnesio-hornblende + Magesio-ferri-hornblende. The margin of error for each mineral category was calculated at a 95% confidence level using the Wilson Score method, taking into account the sample size the success rate in particle characterization and preparing.

Table 6
Width of particles according to their type, APAM = particle from the apical part of an asbestiform mineral, BPAM = particle from the basal part of an asbestiform mineral, DSG = cleavage fragment from an altered mineral, FRAG = cleavage fragment from an unaltered mineral, ASB%= percentage of asbestiform mineral particles, Min-Max = range of width measurements, rieb. = riebeckite, gru. = grunerite, the hornblende category in the table includes magnesio-hornblende, magnesio-ferri-hornblende, IQR = Interquartile Range.

		Asbestiform minerals		Cleavage fragments			Width (μm)			
Mineral	Number	APAM	BPAM	DSG	FRAG	ASB%	Median	Min	Max	IQR
Crocidolite (rieb.)	42	37	0	5	0	88%	0.18	0.06	0.95	0.15
Tremolite	72	29	16	19	8	63%	0.31	0.08	1.12	0.11
Amosite (gru.)	173	113	22	34	4	78%	0.41	0.11	1.25	0.54
Edenite	12	2	1	6	3	25%	0.56	0.38	1.14	0.38
Ferro-actinolite	19	5	5	6	3	53%	0.60	0.17	2.27	0.46
Actinolite	16	2	4	8	2	38%	0.67	0.13	1.78	0.87
Hornblende	18	4	6	7	1	56%	0.71	0.31	2.06	0.42
Anthophyllite	19	3	3	4	9	32%	0.84	0.23	2.29	0.41

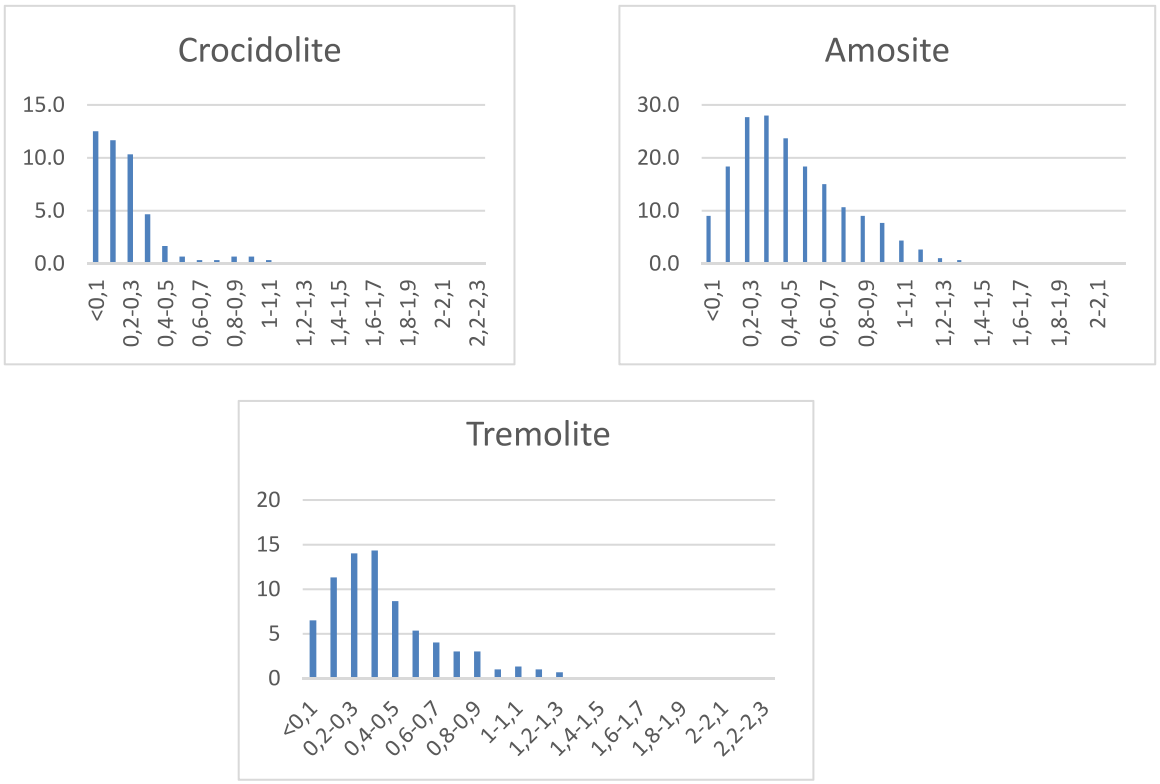

Fig. 5. Width distribution of crocidolite-riebeckite, amosite-grunerite, and tremolite, with the x-axis corresponding to width classes in μm and the y-axis to simple moving averages over 3 values of the number of particles per width class.

thinner on the more magnesian amphiboles (tremolite, anthophyllite, edenite, actinolite, magnesio-hornblende, and magnesio-ferri-hornblende) or that the coating adheres less to these amphiboles and disintegrates during preparation upon contact with oxalic acid. It is the temperature during the contact time with the acid that determines dissolution. An adjustment to preserve a sufficient coating to recognize ABs and NAFBs was carried out only on amosite. A temperature lower than 50°C could potentially increase the recovery efficiency of ABs and NAFBs but may impair the observation of particles at the core of ABs or NAFBs.

Global regulations for the specification of asbestos amphiboles rely on their registration in the CAS registry. However, the molecular and structural formulas of the five asbestos amphiboles have not been specified, unlike those of riebeckite, grunerite, tremolite, and non-asbestos actinolite. Crocidolite from Bolivia is a magnesio-riebeckite, not a riebeckite. The magnesio-riebeckite CF observed here was classified as unregulated in this study.

Particles with DSG morphology can display a high aspect ratio, sometimes exceeding 20. Where this was the case, by convention, these particles were classified as asbestos and included in the APAM group. Due to their increased fragility, it is plausible that a small number of particles classified as DSGs with a similar morphology result from the rupture of these particles with a high aspect ratio.

4.2. Types of particles observed

Regarding the absence of chrysotile, it is possible that the workers selected were not exposed to this type of asbestos. It should be noted, however, that chrysotile is known to be more easily eliminated by the body than amphiboles (Bernstein, 2014; Finkelstein, Dufresne, 1999). Pathologies associated with asbestos exposure generally manifest after a latency period of more than 10 years. This latency varies: 15 years for asbestosis, 20–30 years for pleural plaques, 10 years for pleurisy, 10–15 years for lung cancer, and between 15 and 67 years for mesothelioma (Prazakova et al., 2014). Studies have also revealed the presence of tremolite in commercial products made from chrysotile (Finley et al., 2012 and Compton, Millette, 2021), as well as in the lungs of chrysotile mine workers (Pooley, 1976; Nayebzadeh et al., 2001; Rowlands et al., 1982 and Churg and Wiggs, 1986). It is therefore possible that the chrysotile had been biodegraded and that some of the tremolite particles observed were linked to amphiboles that had polluted the chrysotile. It is also possible that the less acid-resistant chrysotile was dissolved during processing. Since the objective of the study was to detect and identify amphiboles, the resistance of chrysotile to the doses of oxalic acid used was not tested.

Tremolite is less common than actinolite in mainland France due to its less widespread presence in geological formations. However, we observed the opposite in the parenchyma of the subjects involved in this study, with 19% tremolite particles and only 6% actinolite particles. The particle distribution and median width of tremolite were comparable to those of crocidolite and amosite, which are industrial minerals. This distribution was also comparable to that of amphiboles detected in 140 products containing chrysotile (Compton, Millette, 2021). During production, industrial asbestos underwent specific processing to remove impurities, mainly CFs and the shortest fibers. Several patents were filed, mainly at the beginning of the 20th century, and used by manufacturers to perform this operation. This operation was followed by defibration to separate the fibers. As a contaminant of chrysotile, tremolite underwent the same industrial processing as other commercially available asbestos. Furthermore, tremolite is subject to the same geological conditions as chrysotile during the formation of asbestiform minerals. These two phenomena could explain this similarity. It is therefore likely that all or a portion of tremolite particles originate from this source. Tremolite was found alongside talc within the parenchymal samples analyzed in our study in 4 out of 9 cases. Tremolite may be geologically associated with talc (Billon-Galland et al., 2012). However, it seems unlikely that the processing of talc ore after extraction, which mainly involves grinding, is responsible for the distributions observed in

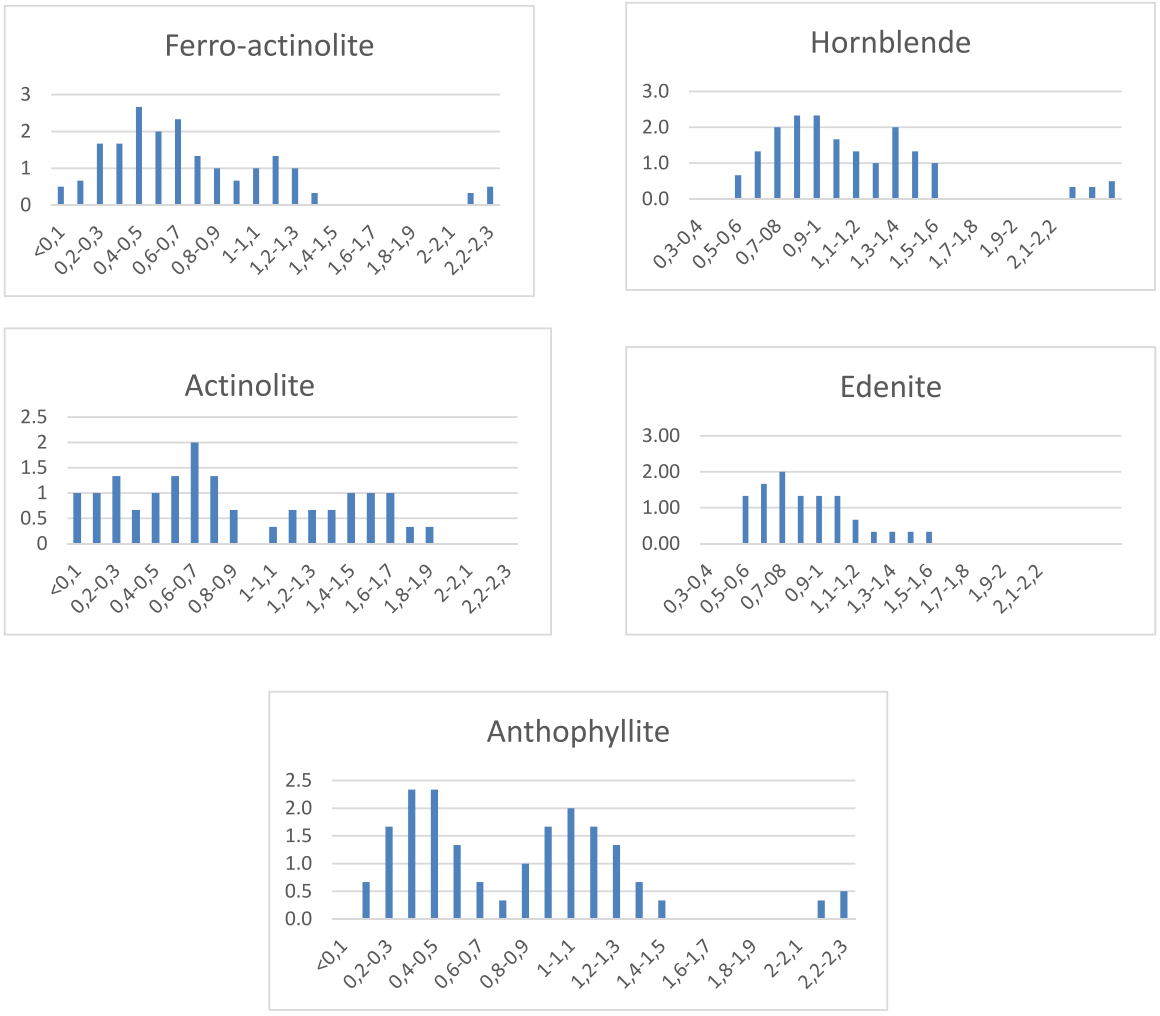

Fig. 6. Width distribution for actinolite, ferro-actinolite, anthophyllite, edenite, and hornblende (magnesio-hornblende+ magnesio-ferri-hornblende), with the x-axis corresponding to width classes in μm and the y-axis to simple moving averages over 3 values of the number of particles per width class.

the parenchyma of the subjects involved in this study.

It is generally accepted that it is rare for asbestos bodies to form around elongate particles less than 10 μm in length (Pooley, 1972), yet 15% of the coated particles in this study were less than 10 μm long. The 7% of coated particles (3 DSGs and 1APAM) with a length less than 7 microns long may have been fractured during sample preparation. If the 3 DSGs had been assigned the length of the longest DSG out of the 6 identified in total of the ABs, only one would be misclassified by convention. The APAM remains correctly classified.

As for uncoated particles, these may also have fractured before inhalation, potentially due to the occupational activities of the patients included in this study, or as they moved through the respiratory system, though this is less likely. Here, only the width distribution was examined. BPAMs originate from the basal portion of asbestiform minerals, and they exhibit a fragility comparable to that of DSGs (altered prismatic amphibole fibers). This similarity results in an overlap in their length dimensions, making it difficult to differentiate them by size. This is explained by the fact that, in nature, the basal portion of an asbestiform amphibole undergoes several fractures, perpendicular to its elongation, sequences during its growing. These fracture sequences are more frequent than those observed in the apical portion (APAM). Consequently, BPAMs exhibit microfractures, which increases their fragility as DSGs (Misseri, 2023).

The 'aspect ratio' within the MBP2022 flowchart is determined based on particle length. The uncertainty associated with particle characterization incorporates potential length variations introduced during sample preparation.

4.3. *Toxicological knowledge*

In vitro (La Maestra et al., 2025) and in vivo (Institut national de l'environnement industriel et des risques, 2025) studies on actinolite and tremolite ASBs and CFs suggest that CFs may be capable of inducing cytotoxic effects, oxidative stress (Reactive Oxygen Species production), and DNA damage in human lung cells (A549) and murine models. In the short term (Day 1), the fibrogenic and carcinogenic potential of CFs appears largely comparable to that of actinolite-asbestos, with seemingly similar cellular signaling pathways (cell adhesion, extracellular matrix, inflammation, vascularization). Both experimental studies suggest that CFs are not rapidly cleared from lung tissue. The Institut national de l'environnement industriel et des risques, 2025) study indicates that at 90 days, the biopersistence of CFs could be at least equal to, or even greater than, that of asbestos. The most notable discrepancies appear over longer periods. The Institut national de l'environnement industriel et des risques, 2025) study suggests that at 90 days, actinolite-asbestos may exhibit greater fibrogenic and carcinogenic potential than CFs, with more persistent inflammation (compared to what appears to be a more transient response for CFs) and more pronounced transcriptomic dysregulation.

Ilgren (2004) and Korchevskiy and Wylie, (2025)) argue that the

observed differences in toxicity could be fundamentally explained by morphology: ASBs tend to be long, thin, flexible, and resistant to dissolution, while CFs are generally shorter, thicker, more brittle, and appear less biopersistent in standard models. Goodman et al. (2023) note that available epidemiological data from cohorts exposed to CFs (taconite miners, gold miners, talc quarry workers) have not demonstrated an attributable excess of mesothelioma. The link between Minnesota taconite miners' exposure to EMP in Mesobi Iron Range and mesothelioma is subject to numerous studies and controversial debate. In a recent case-control study, Shao et al. (2024) found possible evidence of a positive association between mesothelioma and cumulative exposure to Chatfield EMP (width: 0.04–1.5 μm; aspect ratio: 20–1000), Suzuki EMP (width $\leq$ 0.25 μm; length $\leq$ 5 μm) and CFs (aspect ratio $<$ 20) in the worker population. However, it is difficult to find an independent effect regarding the exposure to a mixed aerosol.

An often-underestimated source of divergence concerns the intrinsic variability of CFs based on their geological origin. La Maestra et al. (2025) report notable differences in cytotoxicity and genotoxicity between CFs derived from different rock types (actinolite schist vs. serpentinite vs. amphibole vein), although additional research is needed to fully characterize these differences.

Existing literature on in vivo and in vitro mineral toxicity has frequently relied on a binary classification distinguishing CFs from ASBs, primarily based on dimensional criteria. Such an approach may not fully capture the mineralogical resolution required to interpret surface reactivity. Furthermore, in many experimental studies, the leaching state of the amphiboles is seldom fully characterized. This implies that populations categorized as either CFs or ASBs could potentially represent mixtures of EMPs with heterogeneous surface properties.

4.4. Proposed Classification Framework

The classification proposed here—distinguishing between FRAG, DSG, BPAM, and APAM particles—aims to provide a possible framework to address this limitation. What the literature describes as CFs may, in practice, correspond to FRAG particles, DSG particles, or a combination of both, each potentially carrying different surface chemistries. FRAG particles would expose fresh fracture surfaces dominated by silicon and metal bonds resulting from mechanical breakage, while DSG particles would bear dissolution surfaces from prior hydrothermal leaching, entirely or partially (Vigliaturo et al., 2022) covered by a heterogeneous SIRA (Silica-Rich Amorphous) layer and irregular, amorphous, iron-rich coating. Similarly, particles classified as ASBs may encompass BPAM and APAM populations whose surface characteristics differ substantially: BPAM particles would simultaneously accumulate end-fracture surfaces, dissolution features, SIRA deposits while APAM particles would be dominated by the SIRA nanometric layer, with fracture and dissolution surfaces remaining comparatively rare.

In nature, SIRA layer precipitation on DSGs can correspond to silica residues contained in the hydrothermal fluid during desorption. The presence of these deposits is highly variable. FRAG particles from amphibole grinding, which have not been in direct contact with a hydrothermal fluid or vapor, should not exhibit a SIRA layer. APAM and BPAM particles (from a unidirectionally growing mineral) can be coated with a nanometric SIRA layer, a structure observed in minerals synthesized by a VLC or VLS mechanism (Lee et al., 1999).

Based on crystallization and morphology, the primary purpose of this classification is to clearly distinguish minerals with unidirectional growth from CFs. While its general applicability still requires validation, it already offers a promising framework for characterizing particles in vitro and in vivo, thereby enabling more refined inter-study comparisons.

5. Conclusion

The method used in this study allowed for the precise observation and identification of the particles at the core of ABs and NAFBs, as well as the various uncoated EMP also found in the mineral lung burden. This makes it possible to determine the exact types of EMP to which workers in the mining, quarrying, construction, and public works sectors, as well as farmers, may have been exposed. The focus was specifically on identifying the mineral and characterizing the original habitus of inhaled particles, whether the particle was coated or uncoated.

While amphibole CFs and ASBs share significant physicochemical similarities and exhibit comparable short-term toxicological profiles, long-term exposure data suggests that ASBs may exhibit a more sustained fibrogenic and carcinogenic potential. Consequently, the current binary classification system, which strictly differentiates CFs from ASBs, may present inherent limitations. This dichotomy often overlooks the critical heterogeneity of particles arising from their geological origin, leaching state, and specific surface properties.

To address these analytical gaps, we propose a refined classification framework distinguishing between FRAG, DSG, BPAM, and APAM particles. By shifting the focus from strictly morphological criteria to crystallization history and surface characteristics (e.g., fresh fracture surfaces versus leached dissolution layers), this approach could facilitate a more nuanced understanding of particle toxicity. Although further experimental validation remains essential, this categorization provides a structured basis for standardizing in vitro and in vivo studies, thereby potentially enhancing the accuracy of hazard assessments for EMPs.

Our study, conducted on a small sample of 25 subjects retrospectively recruited, aimed to evaluate the performance of a new analytical method. It revealed the presence of asbestos-like amphibole particle chemically similar to regulated ASBs and CFs of both regulated and unregulated amphiboles. These unregulated amphiboles represent 38% of the whole of amphibole detected. It is therefore justified to investigate their presence in the lung of more cases and to focus on these biopersistent particles in future research to assess their potential impact on health. These cases will be prospectively recruited with occupational and environmental standardized questionary to select only workers from sectors dealing with unregulated amphiboles minerals such as mining, quarrying, public works or agriculture and avoiding any industrial asbestos exposure.

CRediT authorship contribution statement

Jean-Claude Pairon: Writing – original draft, Validation, Resources, Investigation, Funding acquisition, Formal analysis, Data curation, Conceptualization. **Prieur judicael:** Resources, Investigation, Formal analysis, Conceptualization. **Patrick Bontemps:** Resources, Methodology, Investigation, Funding acquisition, Formal analysis, Conceptualization. **Camille Carles:** Resources, Investigation, Formal analysis, Data curation. **Catherine Verdun-Esquer:** Resources, Investigation, Funding acquisition, Formal analysis, Data curation. **Tomas Danek:** Resources, Investigation, Formal analysis, Data curation. **Karine Beugnon:** Resources, Investigation, Data curation. **Sara De Salvo:** Resources, Investigation, Formal analysis, Data curation. **MISSERI Maxime:** Writing – review & editing, Writing – original draft, Visualization, Validation, Supervision, Project administration, Methodology, Investigation, Funding acquisition, Formal analysis, Data curation, Conceptualization. **Laurent Martinon:** Writing – original draft, Validation, Resources, Methodology, Investigation, Funding acquisition, Formal analysis, Conceptualization.

Declaration of Competing Interest

The authors declare that they have no known competing financial interests or personal relationships that could have appeared to influence the work reported in this paper.

Acknowledgments

We would like to extend our warm thanks to André Pauss, without whose help this project would not have been possible, Milia Belacel who managed the coordination with IIMTPIF, Jorge Boczkowski and Nethaajee Ganaserampillai who proofread this manuscript and provided comments that enriched the text. We also thank François Oudet and Caroline Lefebvre from the Physico-Chemical Analysis Service (SAPC) of UTC for their valuable assistance during the control analyses carried out on the TEM Jeol 2100F of UTC.The authors gratefully acknowledge the French Agency for Food, Environmental and Occupational Health and Safety (ANSES) for the financial support with the French National Research Program for Environmental and Occupational Health, project CoFePMAi [grant number 2019/1/098] and the the French Ministry of the Economy, Finance, and Industrial and Digital Sovereignty with the Research Tax Crédit [grant ad-lab CIR 2019-2025].

Data availability

Data will be made available on request.

References

ANSES, 2015. Effets sanitaires et identification des fragments de clivage d'amphiboles issus des matériaux de carrière. Rapp. D. 'Expert. Collect. 218. ⟨https://www.anses.fr/system/files/AIR2014sa0196Ra.pdf⟩.

ANSES, 2017. Particules minérales allongées. Identification des sources d'émission et proposition de protocoles de caractérisation et de mesures. Rapp. D. 'Expert. Collect. 164. ⟨https://www.anses.fr/system/files/AIR2016SA0034Ra.pdf⟩.

Ballirano, P., Skogby, H., Gianchiglia, F., Di Carlo, M.C., Campopiano, A., Cannizzaro, A., Pacella, A., 2022. Chemical and structural characterization of UICC amosite fibres from Penge mine (South Africa): crystal structure of UICC amosite fibres. Period. di Mineral. 91 (2). https://doi.org/10.13133/2239-1002/17767.

Baumann, O., Lacas, F., 2014. L'actinolite asphyxie les chantiers de TP. Le. Monit. ⟨https://web.archive.org/web/20260410152803/https://www.lemoniteur.fr/article/l-actinolite-asphyxie-les-chantiers-de-tp.1442889⟩.

Bernstein, D.M., 2014. The health risk of chrysotile asbestos. Curr. Opin. Pulm. Med. 20 (4), 366–370. https://doi.org/10.1097/MCP.0000000000000064.

Bignon, J., Bonnaud, G., Jaurand, M.C., Goni, J., Dufour, G., 1970. Méthode d'isolement et de concentration des "corps ferrugineux" du poumon humain. leur Fr. équence Et. leur signification. J. Fr. Med. Chir. Thorac. 24, 71–86.

Billon-Galland, M.A., Brochard, P., Dion, C., Dumortier, P., Henrotin, J.B., Herrera, H., Vendel, J., 2012. Evaluation des risques relatifs au talc seul et au talc contaminé par des fibres abestiformes et non abestiformes. Anses.

Bowes, D.R., Farrow, C.M., 1997. Major and trace element compositions of the UICC standard asbestos samples. Am. J. Ind. Med. 32 (6), 592–594. https://doi.org/10.1002/(sici)1097-0274(199712)32:6%3C592::aid-ajim3%3E3.0.co;2-s.

Brouet, G., Bignon, J., Bonnaud, G., Goni, J., Chrétien, J., et Pariente, R., 1967. Calcifications pleurales associées à un empoussiérage asbestosique détecté par l'examen de microprélèvements au microscope polarisant (A propos de deux observations). Extr. du J. Français De. Médecine Et. Chir. Thorac. Tome XXI 2, 181–196 n°.

Campbell, W.J., Huggins, C.W., Wylie, A.G., 1980. Chemical and physical characterization of amosite, chrysotile, crocidolite, and nonfibrous tremolite for oral ingestion studies by the interior (Report of Investigations No. 8452). U. S. Dep. Inter. Bur. Mines.

Capella, S., Bellis, D., Belluso, E., 2016. Diagnosis of asbestos-related diseases: The mineralogist and pathologist's role in medicolegal field. Am. J. Forensic Med. Pathol. 37 (1), 24–28. https://doi.org/10.1097/PAF.0000000000000206.

Castellan, R., Castranova, V., Harper, M., Hearl, F.J., Middendorf, P.J., Stayner, L., Zumwalde, R.D., 2011. Current Intelligence Bulletin 62: Asbestos Fibers and Other Elongate Mineral Particles. State Sci. Roadmap Res. ⟨http://www.cdc.gov/niosh/docs/2011-159/⟩.

Chatfield, E.J., 2018. Measurement of elongate mineral particles: What we should measure and how do we do it? Toxicol. Appl. Pharmacol. 361, 36–46. https://doi.org/10.1016/j.taap.2018.08.010.

Churg, A., 1982. Fiber counting and analysis in the diagnosis of asbestos-related disease. Hum. Pathol. 13 (4), 381–392. https://doi.org/10.1016/S0046-8177(82)80227-X.

Churg, A., Wiggs, B., 1986. Fiber size and number in workers exposed to processed chrysotile asbestos, chrysotile miners, and the general population. Am. J. Ind. Med. 9 (2), 143–152. https://doi.org/10.1002/ajim.4700090205.

Compton, S.P., Millette, J.R., 2021. Quantification of amphibole in chrysotile asbestos-containing products. Asbestos Other Elongate Miner. Part. N. Contin. Chall. 21st Century 341–361. https://doi.org/10.1520/STP163220200054.

Craighead, J.E., Mossman, B.T., 1982. The pathogenesis of asbestos-associated diseases. N. Engl. J. Med. 306 (24), 1446–1455. https://doi.org/10.1056/NEJM198206173062403.

De Vuyst, P., Karjalainen, A., Dumortier, P., Gibbs, A., 1998. Guidelines for mineral fibre analyses in biological samples: report of the ERS Working Group. European Respiratory Society. Eur. Respir. J. 11 (6), 1416–1426. https://doi.org/10.1183/09031936.98.11061416.

Dodson, R.F., Williams Jr,, M.G., Hurst, G.A., 1983. Method for removing the ferruginous coating from asbestos bodies. J. Toxicol. Environ. Health Part A 11 (4-6), 959–966. https://doi.org/10.1080/15287398309530398.

Donaldson, K., Poland, C.A., Murphy, F.A., MacFarlane, M., Chernova, T., Schinwald, A., 2013. Pulmonary toxicity of carbon nanotubes and asbestos—similarities and differences. Adv. Drug Deliv. Rev. 65 (15), 2078–2086. https://doi.org/10.1016/j.addr.2013.07.014.

Dumortier, P., De Vuyst, P., 1988. Object-marking, a bridge between light and analytical electron microscopy for particles characterization. J. Electron Microsc. Tech. 8 (2), 229–230. https://doi.org/10.1002/jemt.1060080213.

Finkelstein, M.M., 2019. Comments on "Dimensions of elongate mineral particles with implications for pathogenicity and classification as asbestiform versus cleavage fragments". Ultrastruct. Pathol. 43 (6), 326–329. https://doi.org/10.1080/01913123.2019.1693457.

Finkelstein, M.M., Dufresne, A., 1999. Inferences on the kinetics of asbestos deposition and clearance among chrysotile miners and millers. Am. J. Ind. Med. 35 (4), 401–412. https://doi.org/10.1002/(sici)1097-0274(199904)35:4<401::aid-ajim12>3.0.co;2-4.

Finley, B.L., Pierce, J.S., Phelka, A.D., Adams, R.E., Paustenbach, D.J., Thuett, K.A., Barlow, C.A., 2012. Evaluation of tremolite asbestos exposures associated with the use of commercial products. Crit. Rev. Toxicol. 42 (2), 119–146. https://doi.org/10.3109/10408444.2011.636028.

Fleiss, J.L., 1971. Measuring nominal scale agreement among many raters. Psychol. Bull. 76 (5), 378.

Germine, M., Puffer, J.H., 2020. Analytical transmission electron microscopy of amosite asbestos from South Africa. Arch. Environ. & Occup. Health 75 (1), 36–44. https://doi.org/10.1080/19338244.2018.1556201.

Givargizov, E.I., 1973. Oriented growth of whiskers and plate crystals of CdSe on CdSe substrates. In: Doklady Akademii Nauk, 211. Russian Academy of Sciences, pp. 332–335.

Gloyne, S.R., 1931. The formation of the asbestosis body in the lung. Tubercle 12 (9), 399–401. https://doi.org/10.1016/S0041-3879(31)80143-6.

Goodman, J.E., Becich, M.J., Bernstein, D.M., Case, B.W., Mandel, J.H., Nel, A.E., Gibbs, G., 2023. Non-asbestiform elongate mineral particles and mesothelioma risk: Human and experimental evidence. Environ. Res. 230, 114578 https://doi.10.1016/j.envres.2022.114578.

Gross, P., Cralley, L.J., deTreville, R.T., 1967. "Asbestos" bodies: Their nonspecificity. Am. Ind. Hyg. Assoc. J. 28 (6), 541–542. https://doi.org/10.1080/00028896709342681.

Gualtieri, A.F., 2018. Towards a quantitative model to predict the toxicity/pathogenicity potential of mineral fibers. Toxicol. Appl. Pharmacol. 361, 89–98. https://doi.org/10.1016/j.taap.2018.05.012.

Gualtieri, A.F., Pollastri, S., Bursi Gandolfi, N., Gualtieri, M.L., 2018. vitro acellular dissolution of mineral fibres: A comparative study. Sci. Rep. 8(1) 7071 4. https://doi.org/10.1038/s41598-018-25531-.

Harper, M., Lee, E.G., Doorn, S.S., Hammond, O., 2008. Differentiating non-asbestiform amphibole and amphibole asbestos by size characteristics. J. Occup. Environ. Hyg. 5 (12), 761–770. https://doi.org/10.1080/15459620802462290.

Harper, M., Lee, E.G., Slaven, J.E., Bartley, D.L., 2012. An inter-laboratory study to determine the effectiveness of procedures for discriminating amphibole asbestos fibers from amphibole cleavage fragments in fiber counting by phase-contrast microscopy. Ann. Occup. Hyg. 56 (6), 645–659. https://doi.org/10.1093/annhyg/mer123.

Hawthorne, F.C., Oberti, R., Harlow, G.E., Maresch, W.V., Martin, R.F., Schumacher, J.C., Welch, M.D., 2012. Nomenclature of the amphibole supergroup. Am. Mineral. 97 (11-12), 2031–2048. https://doi.org/10.2138/am.2012.4276.

Holmes, A., Morgan, A., 1980. Clearance of anthophyllite fibers from the rat lung and the formation of asbestos bodies. Environ. Res. 22 (1), 13–21. https://doi.org/10.1016/0013-9351(80)90114-0.

Ilgren, E.B., 2004. The biology of cleavage fragments: a brief synthesis and analysis of current knowledge. Indoor Built Environ. 13 (5), 343–356. https://doi.org/10.1177/1420326×04047563.

Institut national de l'environnement industriel et des risques. (2025). Étude de la toxicité pulmonaire des fragments de clivage d'actinote comparée à celle de l'amiante actinote (Rapport 4p). ⟨https://www.ineris.fr/sites/default/files/contribution/Documents/2025_Note_%C3%89tude%20de%20la%20toxicit%C3%A9%20pulmonaire%20de%20fragments%20de%20clivage%20d%27actinolite.pdf⟩.

Jung, H.S., Jang, J., Cho, Y., Lee, J.C., Kim, H., 2021. Asbestos in the ambient air from rural, urban, residential, baseball and mining areas in South Korea. Environ. Chem. Lett. 19, 3487–3495. https://doi.org/10.1007/s10311-021-01226-7.

Kohyama, N., Fujiki, M., Kishimoto, T., Morinaga, K., 2017. Lung cancer in a patient with predominantly short tremolite fibers in his lung. Am. J. Ind. Med. 60 (9), 831–838. https://doi.org/10.1002/ajim.22748.

Kohyama, N., Shinohara, Y., Suzuki, Y., 1996. Mineral phases and some reexamined characteristics of the International Union Against Cancer standard asbestos samples. Am. J. Ind. Med. 30 (5), 515–528. https://doi.org/10.1002/(sici)1097-0274(199611)30:5%3C515::aid-ajim1%3E3.0.co;2-s.

Korchevskiy, A.A., Wylie, A.G., 2025. Habit of elongate amphibole particles as a predictor of mesothelial carcinogenicity (Article). Toxicol. Rep. 14, 101908. https://doi.org/10.1016/j.toxrep.2025.101908.

La Maestra, S., Militello, G.M., Alberti, S., Benvenuti, M., Gaggero, L., 2025. Evaluation of the genotoxic and transformation potential induced by asbestos compared to cleavage fragments. Sci. Rep. 15 (1), 3613. https://doi.org/10.1038/s41598-025-86325-z.

Landis, J.R., Koch, G.G., 1977. The measurement of observer agreement for categorical data. biometrics 159–174.
Langer, A.M., Nolan, R.P., Addison, J., 1991. Distinguishing between amphibole asbestos fibers and elongate cleavage fragments of their non-asbestos analogues. Mechanisms in fibre carcinogenesis. Springer US, Boston, MA, pp. 253–267.
Lee, S.T., Wang, N., Zhang, Y.F., Tang, Y.H., 1999. Oxide-assisted semiconductor nanowire growth. Mrs Bull. 24 (8), 36–42. https://doi.org/10.1557/S088376940005288X.
Locock, A.J., 2014. An Excel spreadsheet to classify chemical analyses of amphiboles following the IMA 2012 recommendations. Comput. & Geosci. 62, 1–11. https://doi.org/10.1016/j.cageo.2013.09.011.
McHugh, M.L., 2012. Interrater reliability: the kappa statistic. Biochem. Med. 22 (3), 276–282.
Militello, G.M., Gaggero, L., La Maestra, S., 2021. Asbestiform amphiboles and cleavage fragments analogues: overview of critical dimensions, aspect ratios, exposure and health effects. Minerals 11 (5), 525. https://doi.org/10.3390/min11050525.
Millette, J.R., Compton, S.P., 2005. Asbestos analysis methods. Asbestos. CRC Press, pp. 28–62.
Misseri, M., 2023. Nucleation of naturally occurring calcic amphibole asbestos. Environ. Res. 230, 114940. https://doi.org/10.1016/j.envres.2022.114940.
Misseri, M., Billon-Galland, M.A., 2021. Established cases of the development of asbestos-related lung diseases in miners at the Salau tungsten mine in France due to exposure to asbestos actinolite and asbestos ferro-actinolite. Asbestos and Other Elongate Mineral Particles—New and Continuing Challenges in the 21st Century. pp. 31–61. https://doi.org/10.1520/STP163220200048.
Moulin, E., Yourassowsky, N., Dumortier, P., De Vuyst, P., Yernault, J.C., 1988. Electron microscopic analysis of asbestos body cores from the Belgian urban population. Eur. Respir. J. 1 (9), 818–822. https://doi.org/10.1183/09031936.93.01090818.
Nayebzadeh, A., Dufresne, A., Case, B., Vali, H., Williams-Jones, A.E., Martin, R., Clark, J., 2001. Lung mineral fibers of former miners and millers from Thetford-Mines and asbestos regions: A comparative study of fiber concentration and dimension. Arch. Environ. Occup. Health 56 (1), 65–76. https://doi.org/10.1080/00039890109604056.
Okimoto, Qi, F., Jube, G., Napolitano, S., Pass, A., Laczko, H.I., Carbone, M., 2013. Continuous exposure to chrysotile asbestos can cause transformation of human mesothelial cells via HMGB1 and TNF-α signaling. Am. J. Pathol. 183 (5), 1654–1666. https://doi.org/10.1016/j.ajpath.2013.07.029.
Pairon, J.C., 1996. Approches biologiques pour l'étude de populations exposées à des cancérogènes respiratoires. Doctoral dissertation. Paris 12, 396.
Pollastri, S., D'Acapito, F., Trapananti, A., Colantoni, I., Andreozzi, G.B., Gualtieri, A.F., 2015. The chemical environment of iron in mineral fibres. A combined X-ray absorption and Mössbauer spectroscopic study. J. Hazard. Mater. 298, 282–293. https://doi.org/10.1016/j.jhazmat.2015.05.010.
Pooley, F.D., 1972. Asbestos bodies, their formation, composition and character. Environ. Res. 5 (4), 363–379. https://doi.org/10.1016/0013-9351(72)90039-4.
Pooley, F.D., 1976. An examination of the fibrous mineral content of asbestos lung tissue from the Canadian chrysotile mining industry. Environ. Res. 12 (3), 281–298. https://doi.org/10.1016/0013-9351(76)90038-4.
Prazakova, S., Thomas, P.S., Sandrini, A., Yates, D.H., 2014. Asbestos and the lung in the 21st century: an update. Clin. Respir. J. 8 (1), 1–10. https://doi.org/10.1111/crj.12028.
Rasmuson, J.O., Roggli, V.L., Boelter, F.W., Rasmuson, E.J., Redinger, C.F., 2014. Cumulative Retrospective Exposure Assessment (REA) as a predictor of amphibole asbestos lung burden: validation procedures and results for industrial hygiene and pathology estimates. Inhal. Toxicol. 26 (1), 1–13. https://doi.org/10.3109/08958378.2013.845273.
Ray, R., 2021. The Usefulness and Limitations of Semiquantitative Energy Dispersive Spectroscopy in Asbestos Analysis. In: Millette, J.R., Webber, J.S. (Eds.), Asbestos and Other Elongate Mineral Particles—New and Continuing Challenges in the 21st Century. ASTM International, (West Conshohocken, PA, pp. 31–61. https://doi.org/10.1520/STP163220200048.
Roggli, V.L., Green, C.L., 2019. Dimensions of elongate mineral particles: A study of more than 570 fibers from more than 90 cases with implications for pathogenicity and classification as asbestiform vs. cleavage fragments. Ultrastruct. Pathol. 43 (1), 1–5. https://doi.org/10.1080/01913123.2019.1566298.
Rowlands, N., Gibbs, G.W., McDonald, A.D., 1982. Asbestos fibres in the lungs of chrysotile miners and millers—a preliminary report. Inhaled Part. V. Pergamon 411–415. https://doi.org/10.1016/B978-0-08-026838-5.50032-5.
Shedd, K.B., 1985. Fiber dimensions of crocidolites from Western Australia, Bolivia, and the Cape and Transvaal provinces of South Africa. US Department of the Interior, Bureau of Mines.
Siegrist Jr., H.G., Wylie, A.G., 1980. Characterizing and discriminating the shape of asbestos particles. Environ. Res. 23 (2), 348–361. https://doi.org/10.1016/0013-9351(80)90070-5.
Sunagawa, I., Takahashi, Y., Imai, H., Yamada, S., 2005. Topological whisker bundles of amphibole and frost column of quartz. J. Cryst. Growth 276 (3-4), 663–673. https://doi.org/10.1016/j.jcrysgro.2004.11.412.
Van Orden, D.R., Allison, K.A., Lee, R.J., 2008. Differentiating amphibole asbestos from non-asbestos in a complex mineral environment. Indoor Built Environ. 17 (1), 58–68. https://doi.org/10.1177/1420326×07087006.
Veblen, D.R., Ribbe, P.H. (Eds.), 1981. Amphiboles and other hydrous pyriboles: mineralogy. MSA Rev. Mineral. 9 A, 372.
Veblen, D.R., Ribbe, P.H. (Eds.), 1982. Amphiboles: petrology and experimental phase relations. MSA Rev. Mineral. 9B, 390.
Veblen, D.R., Wylie, A.G., 1993. Mineralogy of amphiboles and 1:1 layer silicates. Rev. Mineral. Geochem 28, 61–138. https://doi.org/10.1515/9781501509711-006.
Vigliaturo, R., Jamnik, M., Dražić, G., Podobnik, M., Žnidarič, M.T., Ventura, G.D., Gieré, R., 2022. Nanoscale transformations of amphiboles within human alveolar epithelial cells. Sci. Rep. 12 (1), 1782. https://doi.org/10.1038/s41598-022-05802-x.
Visonà, S.D., Bertoglio, B., Capella, S., Belluso, E., Austoni, B., Colosio, C., Taioli, E., 2023. Asbestos burden in lungs of mesothelioma patients with pleural plaques, lung fibrosis and/or ferruginous bodies at histology: a postmortem SEM-EDS study. bgad090 Carcinogenesis. https://doi.org/10.1093/carcin/bgad090.
Visonà, S.D., Crespi, E., Belluso, E., Capella, S., De Matteis, S., Filippi, F., Colosio, C., 2022. Reconstructing historical exposure to asbestos: the validation of "educated guesses. Occup. Med. 72 (8), 534–540. https://doi.org/10.1093/occmed/kqac084.
Wagner R.S. and Ellis W.C., Trans. Met. Soc. AIME 426. (1965) 1053.
Wylie, A.G., Korchevskiy, A.A., Van Orden, D.R., Chatfield, E.J., 2022. Discriminant analysis of asbestiform and non-asbestiform amphibole particles and its implications for toxicological studies (Article). Comput. Toxicol. 23, 100233. https://doi.org/10.1016/j.comtox.2022.100233.